Shallow VSP survey using a small vibrator source

Soo K. Miong, Joe Wong, Eric V. Gallant, Robert R. Stewart, and Kevin W. Hall

ABSTRACT

A shallow VSP survey was conducted in the Rothney Test Well using the U of C EnviroVibe as a source and a downhole clamping 3-C geophone in the well. The receiver was placed at depths ranging from 5 m to 90 m at half-metre intervals. Two VSPs were recorded with the vibrator located 15 m and 30 m south of the well head. The three-component data were subjected to wavefield separation and vector rotation to separate P and S waves. Down-doing wavefields, as well as up-going and down-going tube waves, were removed to isolate the P-wave reflections. The residual up-going P-wave reflections were mapped using an approximate VSP/CDP procedure. The reflectivity maps showed good correlation with resistivity, gamma ray, and sonic velocity logs in the well. The experiment confirmed the belief that the EnviroVibe vibrator, when used as a source in near-surface VSP surveys, produces enough high-frequency energy to be effective for imaging relatively thin stratigraphy in the upper 100 m.

INTRODUCTION

The Rothney Test Well is an important part of the Department of Geoscience's teaching and research infrastructure (Wong et al., 2007). It is drilled into the Paskapoo formation on University of Calgary property near the hamlet of Priddis, Alberta. The well is about 125 m deep, and is protected from collapse by 100-mm-ID PVC casing. It has been used for demonstrating well-logging and VSP surveys using a sledge hammer source (Miong, 2008; Miong et al., 2007). This report presents data from two VSPs obtained by using the U of C EnviroVibe vibrator as a source and a clamping 3-C geophone in the Rothney well. The data were processed to isolate up-going P-wave reflections that then were mapped using an approximate VSP/CDP method. The project was conducted in order to evaluate the effectiveness of using shallow VSPs for imaging near-surface stratigraphy. In this case, we were successful in correlating VSP reflection maps to the layered structure of the Paskapoo formation as identified by sonic velocity, resistivity, and natural gamma-ray logs.

ACQUISITION

Figure 1 is a photograph of the EnviroVibe source used in the survey. Figure 2 shows the downhole 3-C geophone that clamps to the well case by means of a motor-driven bow spring.

The first VSP was recorded with the vibrator offset 15 m south of the wellhead. The second VSP was recorded with the vibrator offset 30 m south of the wellhead. In both cases, the downhole 3-C geophone was placed at depths ranging from 5 m to 90 m with half-metre intervals. For both VSPs, the vibrator was driven with frequencies swept from 20 Hz to 200 Hz. The sweep length was 10 seconds, and the listen time was one second. A-to-D conversion, correlation, and recording were done with a single 24-channel Geometrics Geode connected to a Panasonic CF-30 Toughbook computer. The sampling time was 0.5 msec.

Figure 3 shows the VSP seismograms for the 15 m offset, and Figure 4 shows the VSP seismograms for the 30 m offset. Bandpass filtering (using an Ormsby filter with corners at 40-50-200-300 Hz) and AGC have been applied to the seismic traces. The downhole geophone has no azimuth control, so the two horizontal component labels merely indicate two orthogonal orientations. Phase reversals at some depths for the horizontal components were corrected in later processing.

PROCESSING AND ANALYSIS

The two VSPs were processed to yield VSP/CDP maps of P-wave reflections. Figure 5 is a flow chart showing the processing scheme.

Wavefield separation

Wavefield separation is applied to the vertical component VSP gathers to isolate the up-going P-wave reflections. The flow path for this is on the right side of Figure 4 leading to the box labeled Z(up).

For example, Figure 6(a) shows the raw Vertical component seismograms for the 15-m-offset VSP. Median filtering (Stewart, 1984) was used to isolate the down-going first arrivals and other events that have similar down-going velocities. The resulting down-going wavefield, shown on Figure 6(b), was then subtracted from the total wavefield, leaving a difference wavefield. On the difference wavefield, prominent up-going and down-going tube waves were isolated by another application of median filtering. These tube wavefields, shown on Figures 6(c) and 6(d), were subtracted from the difference wavefield, to give a second difference wavefield. On this second difference wavefield, median filtering was applied once again to obtain the down-going shear wavefield shown on Figure 6(e). This was subtracted from the second difference wavefield, yielding the final residual wavefield shown on Figure 6(f). The final residual wavefield consists of mostly up-going reflected P-wave energy, and was used in later processing to create VSP/CDP maps.

Vector rotation for P and S energy

Three-component seismic data gives us an opportunity to maximize the information content and signal-to-noise ratios in the final processed results. If the vector wavefield from a P-wave source is presented as orthogonal components with maximized first-arrival amplitudes in one component, then the component with maximized energy must be parallel to the propagation direction and represents the P wave. The remaining two components, with little or no first arrival energy, represent the transverse or shear waves.

The box on Figure 5 labeled Orientation I denotes the vector rotation of the raw Horizontal 1 and 2 components from Figures 3 and 4. Figure 7 is summarizes what happen in rotating one pair of horizontal component seismograms recorded at one depth. The upper two traces on the left are the raw horizontal-component seismograms. On the right is the hodogram for these traces. The hodogram traces how the direction and amplitude of the velocity vector of the first arrival varies with time in the horizontal plane. The straight line, coincident with the long axis of the hodogram, shows the orientation angle of the two orthogonal horizontal-component geophones with respect to

the propagation direction in the horizontal plane. The values at every time of the two input raw traces can be transformed by a rotation matrix based on this angle. The transformation yields two new seismic traces, one showing maximized energy in the first arrival, and the other showing minimized energy. The hodogram of the new traces will now have its long axis parallel to the x-axis on the hodogram display. The new seismogram, on which the first arrival P-wav energy is maximized, must belong to the component whose vector lies parallel to the horizontal projection of propagation direction of the direct wave.

The results of this analysis applied to the horizontal-component seismograms of the 30-m-offset VSP are displayed on Figure 8. The raw horizontal components of the input seismic wavefield were rotated to yield two orthogonal components with maximized and minimized amplitudes for the first arrivals. The component with maximized amplitudes (H_{max} on Figure 5) is parallel to the radial line joining the well to the vibrator source. The component with minimized amplitude (H_{min} on Figure 5) is transverse to the radial line and should show very little P-wave energy.

Once the maximized horizontal component was found, the same hodogram analysis was applied to it and the vertical component seismogram. Now, however, the rotation takes place in the vertical plane containing the line joining the source location to the geophone location. The procedure indicated by the box labeled Orientation II on Figure 5 operated on the direct arrivals and produced two components H'_{max} and Z'. The direct down-going P-wave energy was maximized on the H'_{max} component, shown on the gather of Figure 9(c). All the features on this gather show apparent velocities in the range 2.5 to 3.0 km/s, the P-wave velocity. We can see from Figure 9(d) that little if any P-wave energy remained in the Z' component (virtually all features on Figure 9(d) have apparent velocities much less than 2.5 to 3.0 km/s). The H'_{max} component was used for first arrival time-picking in preparation for trace alignment and median filtering to remove first arrivals.

A third rotation, represented by the box labeled Orientation III on Figure 5, was applied to the up-going wavefields H_{max}(up) and Z(up). This was a time-variant rotation attempting to further separate P and SV energy in the reflected wavefield. The time variant aspect comes from the possibility that the reflections from different depths arriving at different angles might have had different polarizations. The results on Figure 10 show that the time-variant rotation had very little effect. This is consistent with the observation that, on the input wavefields H_{max}(up) and Z(up), the P and SV energy seemed to be already well-separated.

Deconvolution and Spherical divergence correction

We applied deconvolution to the up-going wavefield Z(up) shown on Figure 10(b). The objective was to enhance frequency content of the primary reflections and to transform the wavelets from the field data to zero-phase wavelets while suppressing multiple reflections. The deconvolution operators were designed using the down-going H'_{max} seismograms with enhanced direct arrivals.

Corrections were made to the amplitudes of the deconvolved Z(up) wavefield to account for spherical divergence. The process consisted of multiplying the amplitude of each time sample by a scalar T^{α}, where T is the recording time and α is a constant coefficient. In the present case, a value of 1.1 for α seemed to account for the spherical divergence reasonably well.

NMO correction

For non-zero offset VSP surveys, a normal moveout (NMO) correction must be applied to the reflection data in order to flatten events. Equations (1) and (2) are used to calculate the time shifts required for the NMO correction for a given receiver at a given depth (see Taner and Koehler, 1969 for details):

$$t^2 = t_{0d}^2 + \frac{x^2}{(\bar{v})^2} , \tag{1}$$

$$t^2 = t_{0r}^2 + \frac{x^2}{(\bar{v})^2} , \tag{2}$$

where t is the time of the reflected event, x is the offset of the source from each receiver, and $\bar{v}$ is the RMS velocity, is used on the first-break picks to get the zero-offset time of the direct arrivals (t_{0d}).

The quantities t_{0d} and t_{0r} are then added to obtain the normal incidence time of the reflected arrivals. The $\bar{v}$ used for the NMO correction is a best estimate value based on the available data, and lies in the range 2.0 to 3.0 km/s. Figure 11 shows the deconvolved Z(up) wavefield data before and after the NMO correction: The up-going reflections are mostly flattened after the NMO correction. Note that Figure 11(a) is plotted in the field-recording time, while Figure 11(b) is plotted in two-way-travel time.

VSP/CDP mapping

In order to show the lateral spatial coverage of the offset VSP surveys, the NMO-corrected wavefields were subjected to VSP/CDP mapping. The standard procedure for VSP/CDP mapping involves ray-tracing through a P-wave velocity model to map the spatial locations of reflections. However, approximate mapping methods such as described by Stewart (1991) can also be used.

The offset x_B of the reflection point from the well for a P-wave arrival over a homogeneous single-layered earth is given in Gulati et al. (1997) as

$$x_B = \frac{x}{2}\left[\frac{vt_v - 2z}{vt_v - z}\right] , \tag{3}$$

where x, v, t_v, z, are the source-receiver offset, constant velocity of the homogeneous single-layered medium, normal incidence time of reflection, and depth of the receiver respectively. This equation is valid for a single-layered earth, but it can be adapted to a

multilayered earth by simply substituting the stacking velocity $\bar{v}$ (assumed equal to RMS velocity) in place of the constant velocity v (Gulati, 1998).

Using the approximate method, final VSP/CDP maps for both the 15-m-offset and 30 m-offset VSP data were produced. They are shown on Figure 12. They are displayed again on Figure 13 to emphasize their correlation with a corridor stack and synthetic seismograms based on the sonic velocity log in the well. On Figure 14, we show the correlation of the VSP/CDP maps with resistivity, P-wave sonic velocity, and natural-gamma ray logs from the well. Also shown is the lithology and stratigraphy as interpreted qualitatively from the gamma ray log. The time-to-depth conversion in VSP/CDP maps was done by applying an RMS velocity of about 2.2 km/s to one-way travel time.

SUMMARY AND DISCUSSION

The 3-C VSP survey in the Rothney Test Well using the EnviroVibe vibrator as a source and the analysis of the resulting field data proved to be very successful. Excellent quality data enabled us to apply sophisticated processing techniques that produced good-quality VSP reflection images. These images correlated well with the stratigraphy encountered in the borehole. This correlation is gratifying, since it is generally quite difficult to use reflection techniques to image thin beds in the upper 100 meters.

Wavefield separation and component rotation methods gave us wavefield components that emphasized shear wave arrivals. It is easy to estimate an average shear-wave velocity in the range 700 to 1000 m/s from the gathers shown on Figure 6(e) and Figure 9(d). These values are consistent with values obtained by Al Dulaijan (2008) using multi-channel analysis of surface waves and shear wave refraction.

ACKNOWLEDGEMENTS

We thank the sponsors of the CREWES Project and NSERC for supporting this research. We are grateful to for GEDCO giving us permission to make extensive use of the VISTA seismic data processing package.

REFERENCES

Al Dulaijan, K., 2008, Near-surface characterization using seismic refraction and surface-wave methods: M.Sc. thesis, University of Calgary.

Gulati, J.S., Stewart, R.R., Preon, J., and Parker, J.M., 1997, 3C-3D VSP: normal moveout correction and VSPCDP transformation: CREWES Research report, **9**.

Gulati, J.S., 1998, Borehole seismic surveying: 3C-3D VSP and land vertical cable analysis: M.Sc. thesis, University of Calgary.

Miong, S.K., 2008, Borehole Geophysical Methods for Near-surface Characterization: M.Sc. thesis, University of Calgary.

Miong, S.K., Stewart, R.R., and Wong, ,J., 2008, characterizing the near surface with VSP and well logs: CREWES Research Report, **19**.

Stewart, R.R., 1991, Rapid map and inversion of P-SV waves: Geophysics, **56**, 859-862.

Taner, T.M. and Koehler, F., 1969, Velocity spectra-digital computer derivation and applications of velocity function: Geophysics, **34**, 859-881.

Wong, J., Miong, S.K., Gallant, E.V., Bentley, L.R., and Stewart, R.R., 2007, VSP and well logs from the U of C test well, CREWES Research Report, **19**.

FIG. 1. The EnviroVibe vibrator source used in the VSP survey.

FIG. 2. The downhole 3C geophone with motor-driven, bow-spring used clamp.

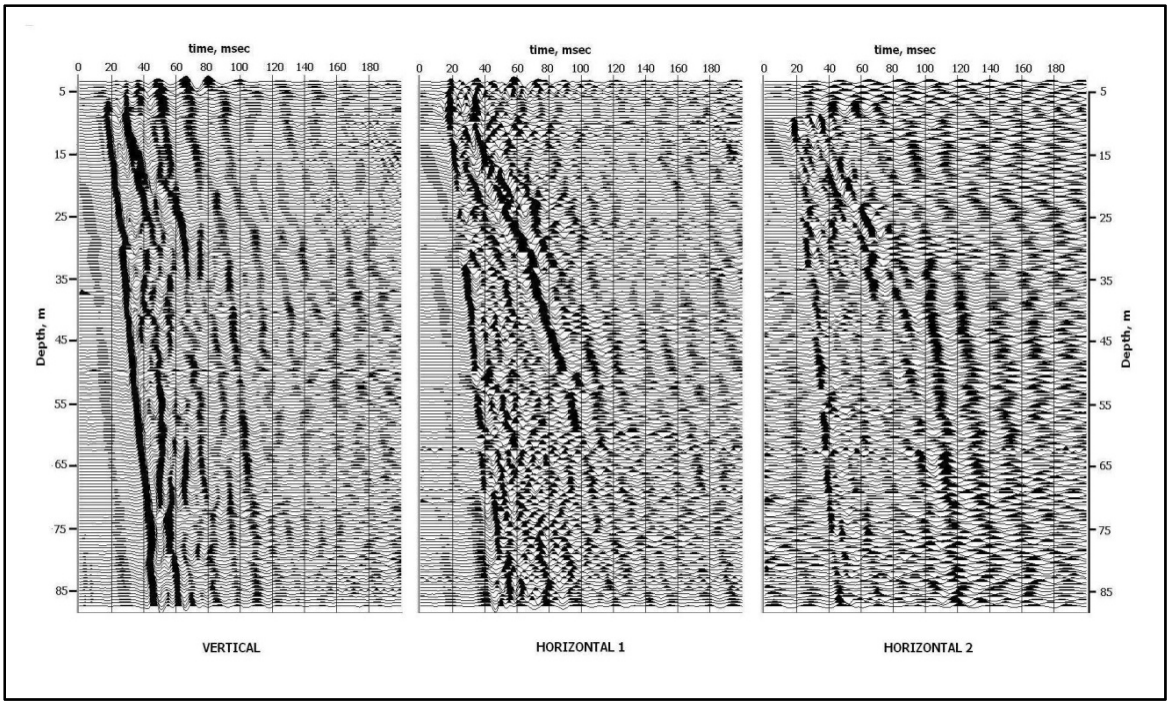

FIG. 3. Field seismograms from 3-C VSP survey with source-to-well offset of 15 m.

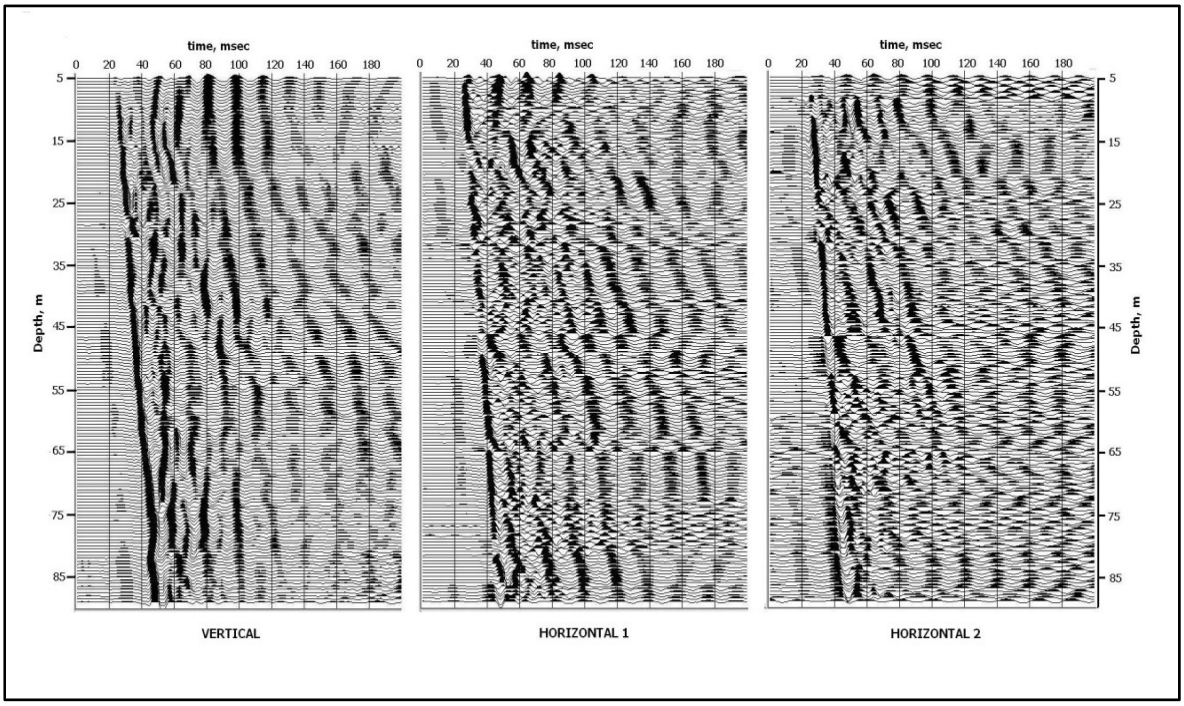

FIG. 4. Field seismograms from 3-C VSP survey with source-to-well offset of 30 m.

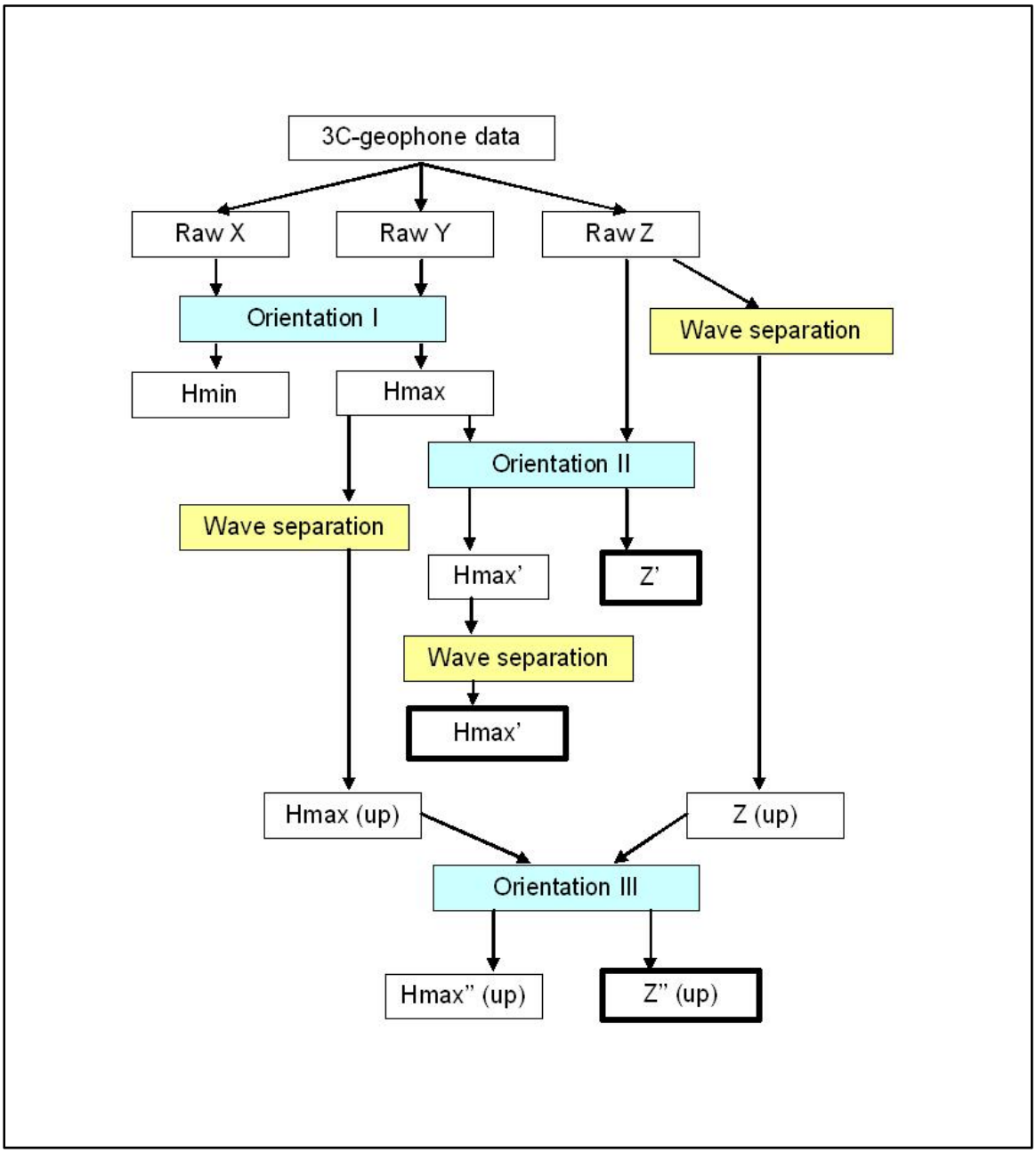

FIG. 5. Processing flow chart showing main wavefield separation and component-rotation (orientation) operations. The primed labels do not refer to vertical or horizontal components, but rather to maximum orthogonal components (Hmax' and Hmax'') and minimum orthogonal components (Z' and Z"") after rotation.

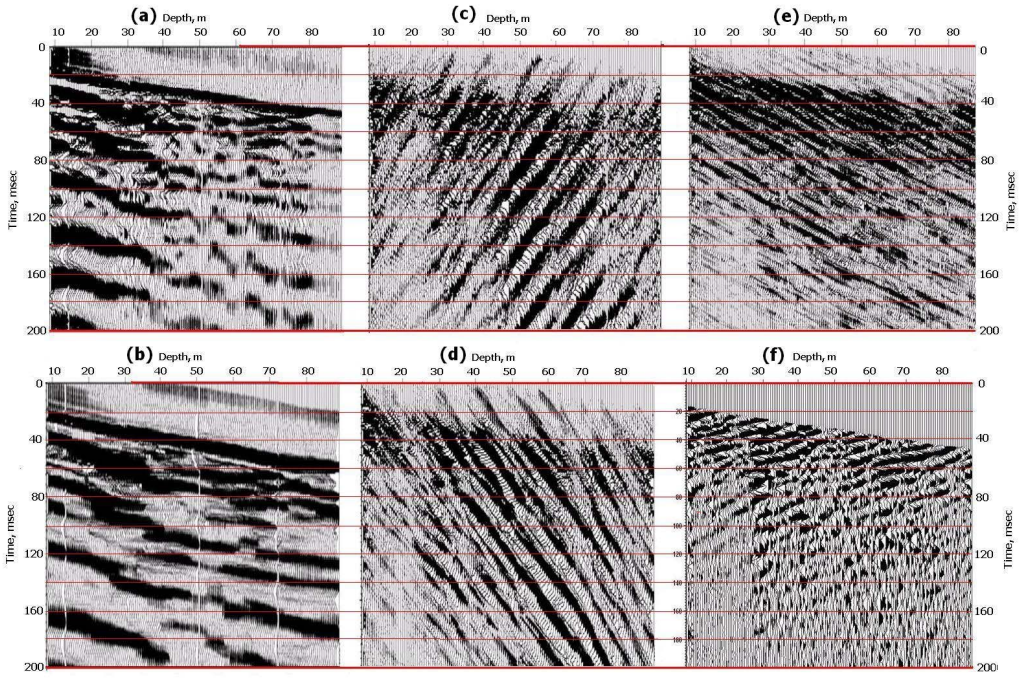

FIG. 6. Various partial wavefields obtained by median filtering the 15-m-offset VSP data: (a) raw vertical component; (b) down-going direct arrival wavefield; (e) and (d) low-velocity tube waves; (e) The down-going S wavefield; (f) final residual wavefield, with mostly up-going reflected P-waves, is labeled as Z(up) on Figure 5.

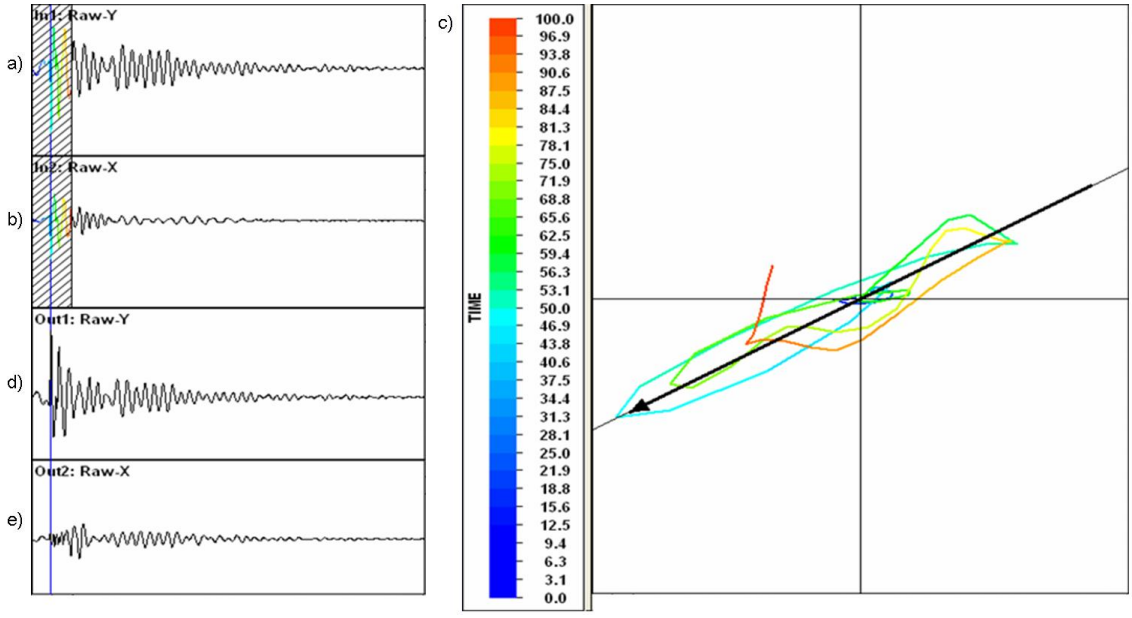

FIG. 7. Hodogram analysis and component rotation using single seismograms form the Horizontal 1 and Horizontal 2 fathers of Figure 3. Color scale refers to percent into the shaded time window on the upper left.

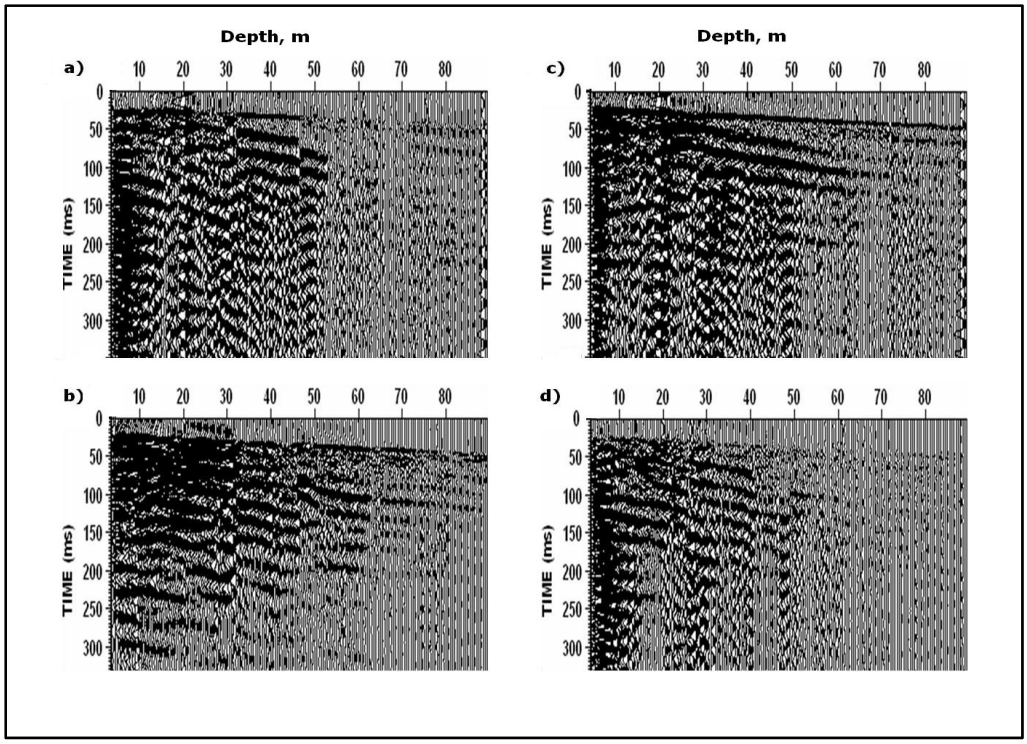

FIG. 8. Horizontal component rotation of the 30-m-offset VSP data (Orientation I on the flow chart of Figure 5): (a) and (b) raw orthogonal horizontal components; (c) maximum orthogonal component H_{max}; (d) minimum orthogonal component $H_{min.}$

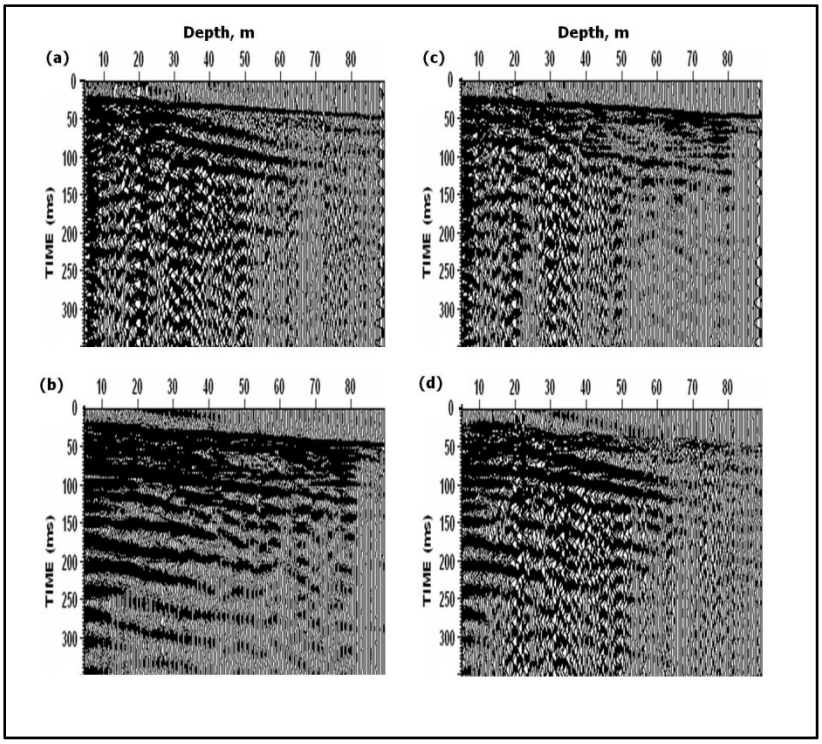

FIG. 9. Orientation II rotation of 30-m-offset data to maximize the down-going wavefield: (a) input H_{max}; b) input Z; c) output H'_{max} with maximized direct P-wave energy; d) output Z'..

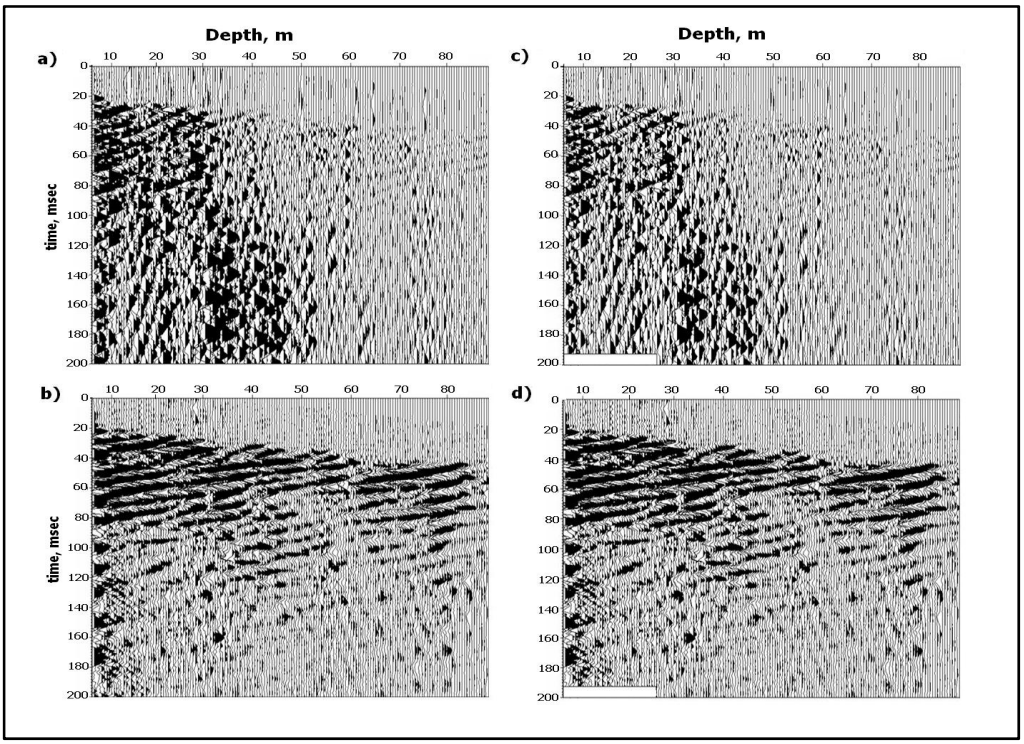

FIG. 10. Orientation III: time-variant rotation of 30-m-offset data to separate P and SV reflections; (a) and (b) Input up-going wavefield H_{max} (up) and Z(up); (c) and (d) output wavefield H''_{max} and Z''. There is very little difference between the input and output wavefield.

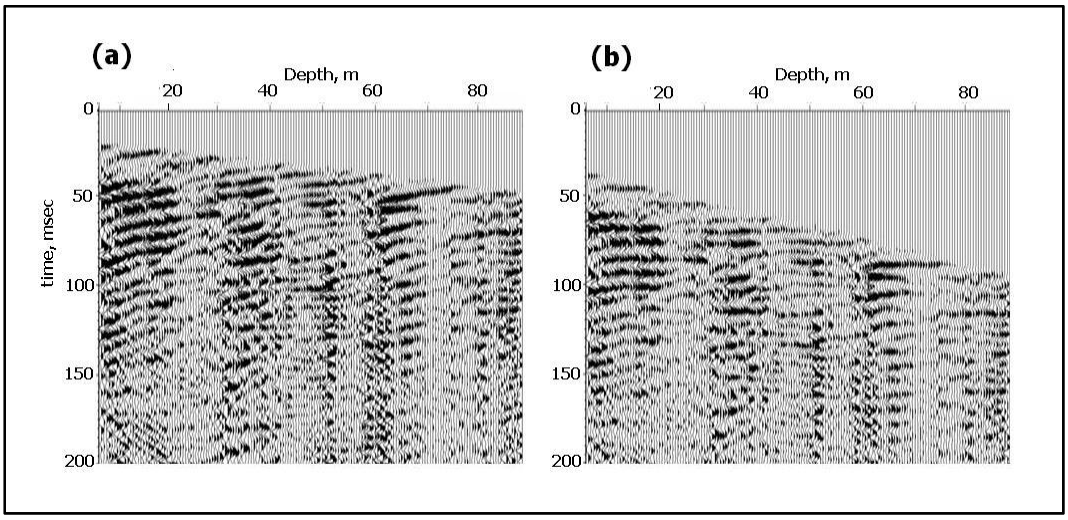

FIG. 11. Up-going P reflected wavefield, deconvolved and corrected for spherical divergence: (a) before, and (b) after NMO correction. The reflections are mostly flattened after NMO correction.

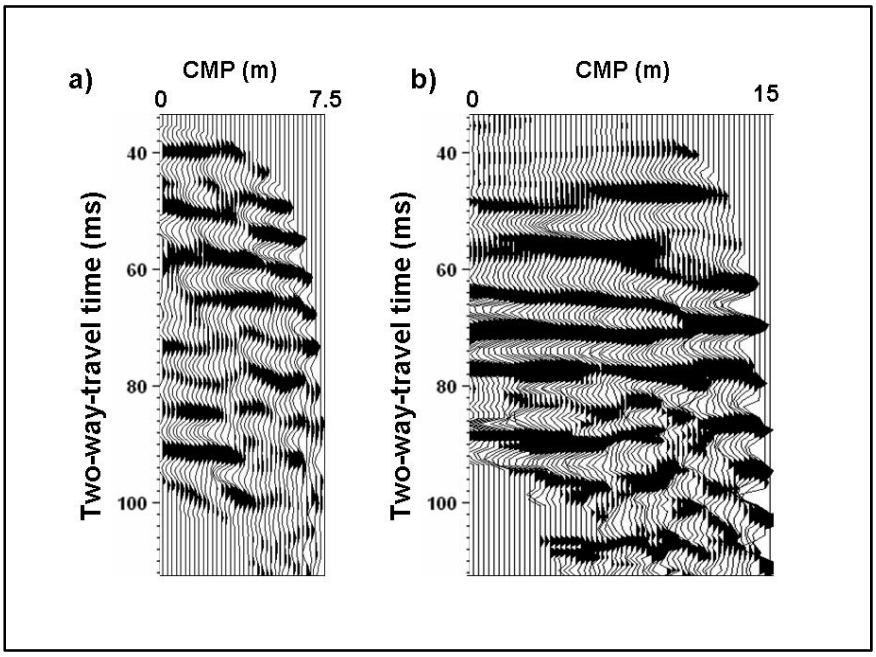

FIG. 12. VSP/CDP maps for (a) 15-m-offset VSP, and (b) 30-m-offset VSP.

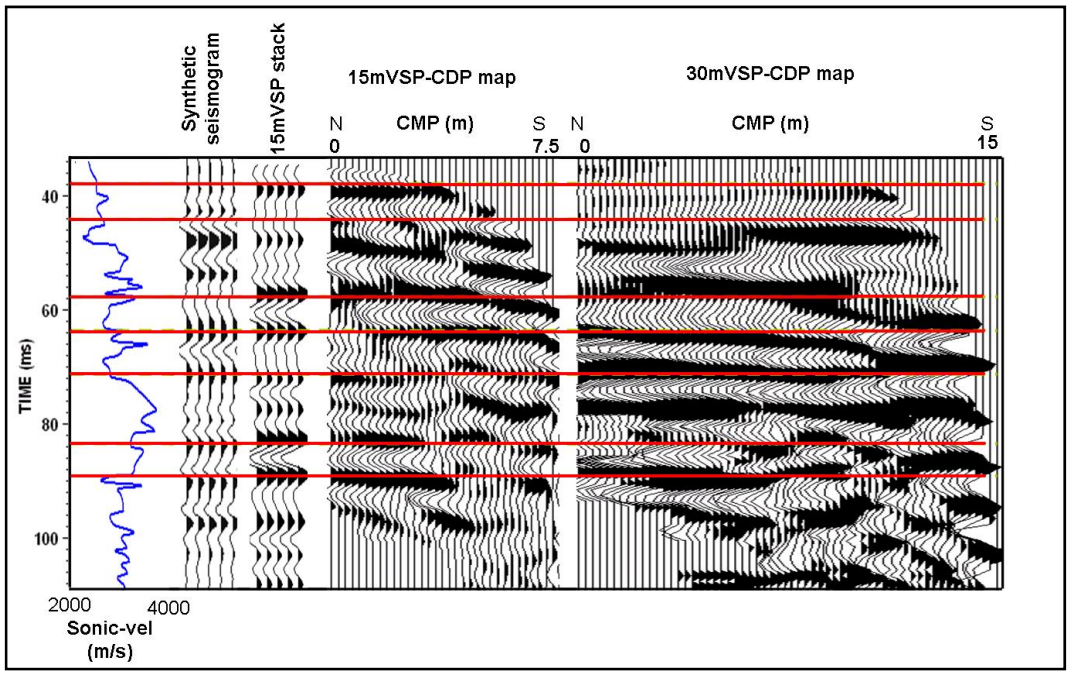

FIG. 13. Correlation of the VSP/CDP maps with sonic velocity log, synthetic seismograms, and corridor stack.

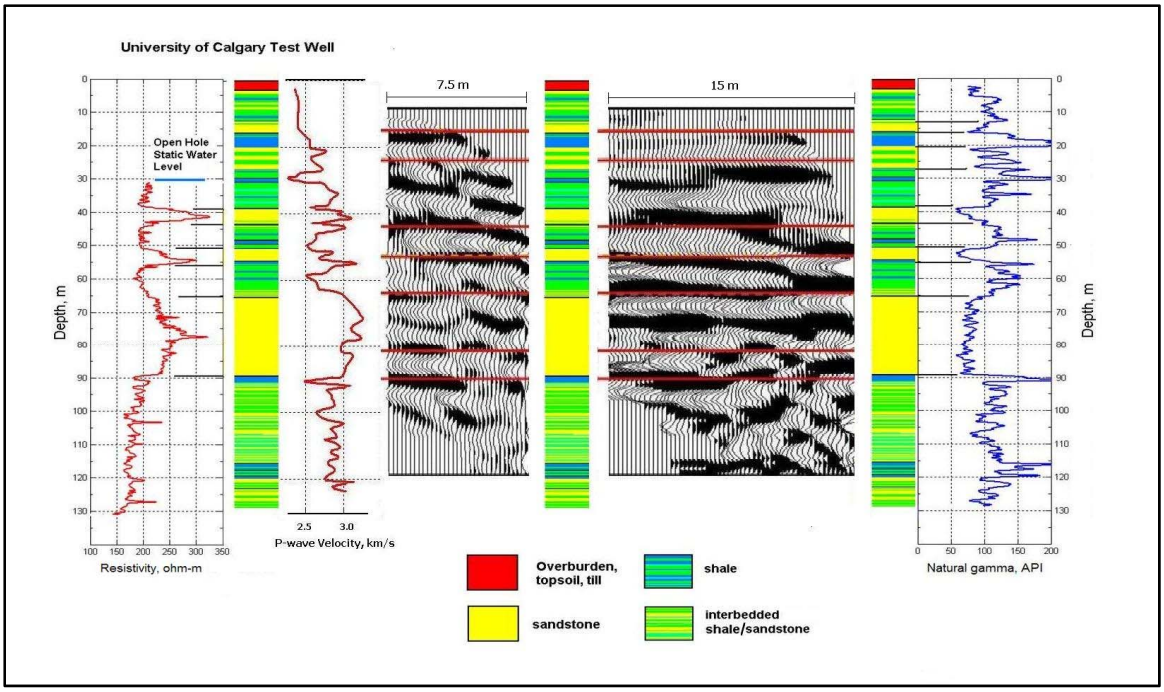

FIG. 14. Correlation of the VSP/CDP maps with well logs and litohology. The lithology was interpreted qualitatively from the natural-gamma ray log on the right.